New Journal and we have not received input yet 23 (2021) 100858

Contents lists available at ScienceDirect

Thermal Science and Engineering Progress

journal homepage: www.sciencedirect.com/journal/thermal-science-and-engineering-progress

Techno-economic assessment of a rotary kiln shell radiation waste heat recovery system

José J. Fierro [a], César Nieto-Londoño [a,*], Ana Escudero-Atehortua [a], Mauricio Giraldo [b], Hussam Jouhara [c], Luiz C. Wrobel [c]

[a] Escuela de Ingenierías, Universidad Pontificia Bolivariana, Medellín, Colombia
[b] Cementos Argos, Medellín, Colombia
[c] College of Engineering, Design and Physical Sciences, Brunel University London, London, UK

ARTICLE INFO

Keywords:
Clinker kiln
Radiation waste-heat recovery
Organic Rankine Cycle
Exergo-economic analysis

ABSTRACT

In this work, the feasibility of implementing a waste heat recovery system based on the capture of radiation emitted from the surface of a rotary kiln is evaluated by coupling CFD analysis and process modelling including mass, energy, and exergy balances. It is found a potential heat recovery of up to 4980 kW of heat with an annulus absorber panel which extends 30 m of the kiln length and reaches an average temperature of up to 240 °C. Such heat could be used to generate 864.25 kW_e of electricity through a Recuperated ORC with a thermal efficiency η_{th} = 17.35% and an exergetic efficiency η_{exg} = 48.62% for a total saving of 16.6 MJ_e per tonne of clinker. An economic feasibility for this recovery alternative is highly dependent on the electricity price in the cement plant location. It is observed for markets with electricity prices exceeding 0.1 $/kWh, the return on investment could reach values of 5% corresponding to a *NPV* close to 0.06 MUSD.

1. Introduction

The cement industry is known for its energy-intensive processes and large flows, therefore is prone to have significant heat losses to the environment, mainly by convection and radiation through the exposed surfaces [1]. Those losses could be recovered as low temperature heat for other applications in the plant facilities [2–4], potentially combined with a thermal storage unit to smooth down fluctuations in the waste heat harvesting [5]. According to [6], inefficiencies in the process showed themselves as higher fuel consumption and higher CO_2 emissions and higher production and environmental costs. Therefore, exploring the use of non-conventional waste energy sources like the heat lost from the kiln surface, which represents up to 15.11% of the input energy [2], could contribute to enhance the cement plant performance and competitiveness. The literature, however, is not as extensive regarding the energy released from the surface of the rotary kiln and the mechanisms to be recovered, due to the difficulties in the actual physical arrangement of a waste heat recovery system based on such a type of waste heat from large non-insulated rotating surfaces. Despite this, some interesting works are presented ahead.

An analysis of the parameters affecting the energy consumption of a rotary kiln in a cement plant in Gaziantep, Turkey, was conducted in [7] estimating that 12.5 MW of energy were lost from the surface of the kiln, accounting for 11.3% of the total energy input to the unit. Specific energy consumption for clinker production (3735.45 kJ/kg) and the anzast layer (i.e., mantle inner lining protective shell) effect were determined to show that the formation of the latter accompanied by the use of high quality magnesia spinel and high alumina refractory bricks provide 7.27% energy savings (271.78 kJ/kg) also bringing up reductions in the CO_2 emissions equivalent to 1614.48 tons per year. In [8] an integrated model is presented to estimate the coating thickness in the burning zone of a rotary cement kiln by using measured process variables and scanned shell temperature ($T\sim$ 150–310 °C). The steady-state one-dimensional model predicts the internal temperature profile along the kiln ($T\sim$ 750–1400 °C) based on the balance equations of a plug flame model burning gas or fuel oil. Then, by considering the temperature gradient between the internal zones and the shell it estimates the formed coating thickness with an absolute error of 3.26 cm or less when compared to a commercial cement kiln. A similar work is presented in [9] where a blocked-off region approach is used in the numerical simulations of radiation and momentum to estimate the impact of the coating layer in

* Corresponding author.
E-mail addresses: jose.fierro@upb.edu.co (J.J. Fierro), cesar.nieto@upb.edu.co (C. Nieto-Londoño), ana.escudero@upb.edu.co (A. Escudero-Atehortua), mgiraldogir@argos.com.co (M. Giraldo), hussam.jouhara@brunel.ac.uk (H. Jouhara), luiz.wrobel@brunel.ac.uk (L.C. Wrobel).

https://doi.org/10.1016/j.tsep.2021.100858

Available online 8 February 2021

Nomenclature

Parameter

T	Temperature [°C]
η	Efficiency
$\dot{I}$	Exergy destruction rate [kW]
EDF	Exergy destruction factor
VFR	Volumetric flow ratio
SP	Size parameter [m]
$\dot{Q}$	Heat flow [kW]
$\dot{W}$	Work [kW]
i	Rate of return [%]
NPV	Net present value [*MUSD*]
PB	Payback time [y]
c	Average unit cost [$/kWh]

Subscript

$_e$	electricity
$_{film}$	film
$_{amb}$	ambient
$_{KS}$	kiln shell
$_{abs}$	absorber
$_{ref}$	reference
$_{cond}$	condenser
$_{th}$	thermal, first law
$_{exg}$	exergetic, second law
$_{tot}$	total

Abbreviations

KS	Kiln shell
VB	Vortex breaker
S2S	Surface to surface
HF	Heat flow
IHE	Internal Heat Exchanger
MUSD	Million dollars

rotary cement kilns.

A numerical modelling of a rotary cement kiln with improvements to shell cooling is carried out in [10]. The one-dimensional model developed enables to take into account the effects of shell-cooling fans via a composite resistance and a forced convection model. The inclusion of the latter provides a significant effect on the accurate portrayal of the predicted shell temperature profile and it also brings down the estimation error by more than 20% in comparison to ignoring these effects. In [11] a waste heat recovery system based on interconnected heat exchangers that are distributed along several regions of the rotary kiln is evaluated. Design requirements, as shell temperature (T 200–350 °C) and required shell heat loss (71–194 kW), are defined for nine regions of the kiln. Then, a performance optimisation of the heat exchangers is executed using the total heat transfer area of the system as the minimisation parameter achieving a 15.6% reduction in the optimal case.

In [12–14] a study was held in a cement production facility in Aalborg, Denmark. Initially, an arc-absorber panel was proposed to recover heat from the radiation of the iso-thermal outer shell (±500 °C) of a rotary kiln. The numerical simulations were performed in 2D using a finite volume approach and a surface to surface (*S2S*) model for radiation and taking into account both the steady and unsteady regimes of flow. An analysis with constant heat flux instead of constant temperature was run to prevent hot-spots on the surface of the rotary kiln and thus guaranteeing safety. Then the absorber was enhanced to an annular shape that allowed the radiation harvesting from all the cylinder surfaces. The panel was subsequently attached to a thermo-electric generator (TEG) based on Zn_3Sb_4, laboratory tests were driven, and it was found that the outlined TEG recovery system produced between 86.78 and 105.91 W/m^2 to an investment cost ranging from 17.56–20.32 $/W and a payback time of 3.58 years.

This work focuses on presenting, based on plant data and numerical simulations, the technical and economic analysis of a heat recovery system based on the capture of radiation emitted by the surface of the rotary kiln shell through an absorber panel. Once captured, such waste heat is used to drive a power generation cycle, specifically a Recuperated ORC. The system, seen as a whole, is economically evaluated to determine its feasibility based on the energy cost of the place where it will be located. Initially, in Section 2 and Section 3, the description of the case study, the modelling procedure and the cross-validation of the CFD simulations are carried out to determine the potential heat to be captured by the absorber panel. Then, in Section 4, the influence of the geometric parameters that affect the amount and quality of the captured waste heat are explored. Next, in Section 5, a consolidation of the harvested heat is presented, and starting from Section 6, it is used for the generation of electricity. The economic figures of the proposed waste heat recovery system, which closes this analysis, is presented in Section 7.

2. Case study

The rotary kiln is a cylinder 4.6 m in diameter and 68 m long, and it is the heart of the clinker production with internal temperatures $T > 1400$ °C in the burning zone, which extends up to 50 m from the flame burner. However, due to safety reasons, the kiln surface is not insulated since it is necessary to verify through visual inspection the appearance of hot spots that could put the operation at risk, namely, potentially melt the shell, i.e., when there are failures in the layer of refractory material inside the kiln compromising its structural integrity. As a result of the lack of insulation, the exterior surface of the kiln shell reaches temperatures as high as $T\tilde{}$ 375 °C and constantly transfers heat by convection and radiation to the environment. It must even be actively cooled in some areas using fans when natural convection appears to be insufficient.

To access such energy loss it is desired to install a suitable heat recovery system that properly meets the challenges that a traditional cooling arrangement could introduce, that is, the technical difficulties of arranging the shell-cooling systems next to a rotating surface and the subsequent visual obstruction. To do so, the most appropriate heat transfer mechanism is radiation, and, in this sense, works such as [12,14,13] have been carried out, where a concentric metallic panel is arranged to capture the radiation emitted by the surface of the kiln without coming into direct contact. The amount of radiation that is available for its harvesting is obtained through a 2D CFD model where fluid dynamics of the surroundings is coupled to the heat transfer calculations. Finally, the recovered heat could be used to produce electricity through a Recuperated ORC. All transport equations are solved using Ansys Fluent 2020 R1. Material, energy and exergy balances are assisted with Aspen Plus V.10 software while the Aspen Process Economic Analyzer (APEA) is used for costing.

3. Absorber panel modelling

In this work the methodology proposed in [12] is used to determine the incident radiation on the panel through steady-state 2D CFD simulations. Radiation is assessed according to the *S2S* model that relies solely on geometric information of the surfaces to calculate the view factors and then compute net radiative exchanges between surfaces that are used as input for heat transfer calculations. It has been used

successfully in different applications where the heat transfer is dominated by radiation like in furnaces [15–17], fire modelling, and solar collectors [18,19], among others, as well as in previous kiln surfaces, considered as heat harvesting systems [12,14,13]. Due to its relatively low computational cost there are attempts to improve its performance i. e. when complex heat transfer situations are assessed, like in material forming where conduction, radiation and convection coexist in the same domain, like in [20]. The *S2S* model requires a much larger computational domain than the interacting surfaces since it neglects the absorption of radiation by the medium. Such a domain is defined conveniently in terms of the diameter of the kiln, as presented in Fig. 1. The absorber panel consists of a cylindrical cap when viewed in 3D or an arc for 2D simulations, concentric to the kiln. It is separated from the kiln surface a distance such that smooth operation is allowed; it is located in a position relative to the vertical axis and from there extends to a fixed span, for cross-validation, of 90°. The panel extends along with the kiln length in sections, which for convenience in presenting the information are usually considered 5 m long, and may or may not have the presence of vortex breakers at the tips as shown in Fig. 2. The effect of positioning parameters is explored later in Section 3.2.

The transport equations, RANS, are solved using the Ansys Fluent 2020 R1 software. As it is a radiation problem, it is not only necessary to use the continuity and momentum equations in the 2D domain. In order to activate the energy equation and the calculation of the view factors between the radiating surfaces, the solution for the steady-state was reached with the coupled approach and the pseudo-transient method, and the under relaxation parameters are tuned to enhance the rate of convergence while the applied turbulence model is the $k-\omega$ *SST*. On this and the convergence criteria of the simulations, we go into detail in Section 3.2.

3.1. Boundary conditions

The computational domain portrayed in Fig. 1 shows a lateral inlet of air which is defined with its nominal velocity at ground level conditions and ambient temperature. Turbulence parameters of such boundary are tuned iteratively to comply with the cross-validation procedure, shown ahead, and finally settled in 15% for the turbulent intensity and 0.001 m in the case of the turbulent length scale. For this entry point, properties of the fluid such as the specific heat and the thermal conductivity are set as constant while the viscosity is estimated through the Sutherland correlation. Top, bottom, and outlet zones work under outflow boundary conditions while the kiln shell and the absorber panel faces are treated like walls with the kiln shell rotating in counter clock motion.

The absorber panel is modelled as a 2.54 cm thick aluminium metallic sheet with a thermal emissivity of 1, assuming it would be painted black, while the kiln surface presents an emissivity of 0.81 for the reference and of 0.87 for the case study, according to the material data sheet. A summary of the boundary conditions is placed in Table 1.

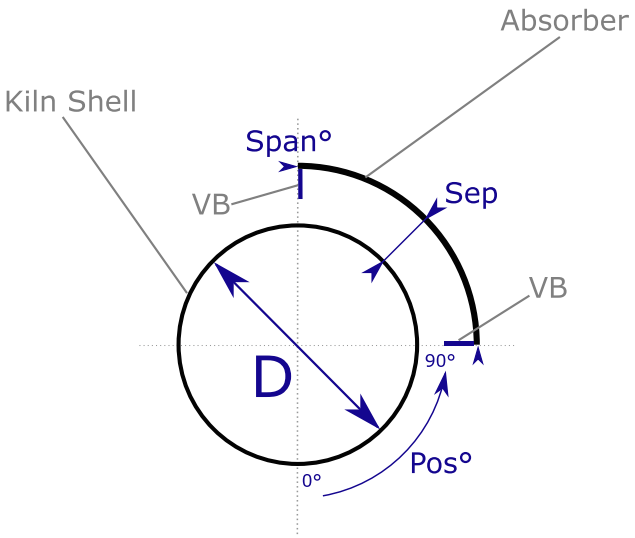

Fig. 2. Close up view of the absorber panel.

3.2. Cross-validation

Cross-validation of the numerical data is then necessary to ensure confidence in the results achieved when varying the boundary conditions to the current case study. This is done by replicating the simulation setup used in the reference [12], as shown in Table 1, and comparing the reported results with the ones obtained in the present work. CFD

Table 1
Simulation setup, reference vs case-study.

Location	Parameter	Reference [12]	Case-study
Kiln	Speed [rpm]	−5	−4
	Shell Temperature (Max) [°C]	500	375*
	Shell Emissivity	0.81	0.87**
Absorber Panel	Position [Degrees]	75	75
	Separation [m]	0.7	0.7
	Span [Degrees]	90	90
Ambient Air	Vel [m/s]	5.86	2.5
	Po [atm]	1	1
	To [°C]	5	27.8
	Tfilm [°C]	252.5	201.4

* Measured using infrared pyrometer.
** According to material data sheet.

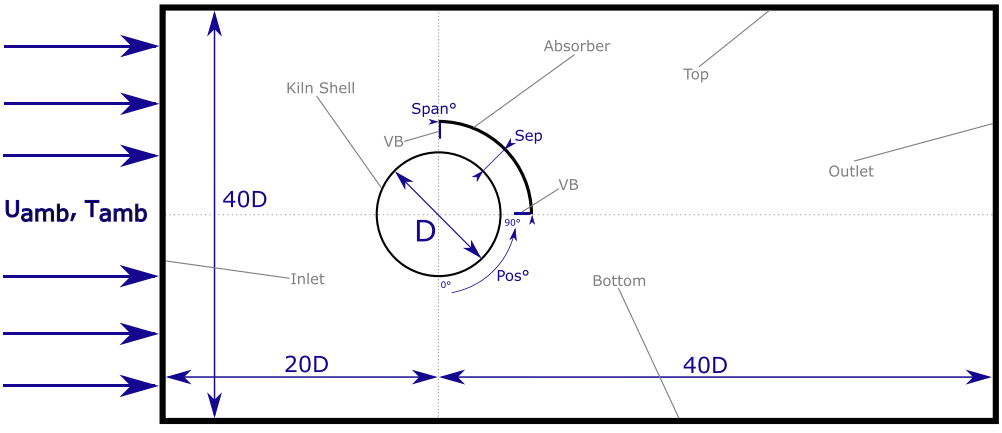

Fig. 1. Computational domain of the 2D simulation. Image adapted from [12].

simulations have several stages of tuning and adjustment that are certainly dependent on the case. However, convergence should not be influenced by any kind of noise, understood as variations in the grid or the residuals. For this reason, convergence criteria are set in two complementary ways, either complying with the absolute criteria of the residuals shown in Table 2 or when the coefficient of lift and drag flatten, which is reached in less than 5000 iterations.

The simulation setup uses fluid properties at film temperature, T_{film}, calculated in Equation 1, as reference values for the lift and drag coefficient estimations since it is a valid approximation of the actual heat transfer temperature.

$$\mathrm{T_{film}} = \frac{T_{KS} + T_{amb}}{2} \tag{1}$$

To guarantee proper heat transfer estimations, a non-structured mesh approach is selected to ensure that the boundary layer is solved with sufficient resolution, that is, with a grid size near the walls where the Y^+ parameter is kept as close as possible to $Y^+ \simeq 1$ on all surfaces through mesh inflation and further refinement. $k-\omega$ *SST* model is the one applied for turbulence in the current simulations since it combines the $k-\omega$ formulation in the inner parts of the boundary layer, allowing the proper estimation of heat transfer near the wall, while switching to a $k-\epsilon$ behaviour in the free-stream, therefore, avoiding the common $k-\omega$ problem that makes the model too sensitive to the inlet free-stream turbulence properties [21]. This model is also the one used in [12].

Finally, a grid independence test is used to select the more advantageous average grid size in terms of computational cost and reliability. Fig. 3 shows the maximum kiln shell temperatures curves for the reference simulation and the current case-study setup. This variable is selected for safety reasons, as it is the maximum advisable operating point for the shell. Although in the reference this temperature is higher, the treatment given in the numerical simulation is the same, with only a small effect on the potential heat transfer being foreseeable. An average grid size of 0.36 m is selected for both sets of simulations as it meets the $Y^+ \simeq 1$ and there is no further change in the average temperature of the absorber panel. The number of mesh elements is larger for the simulations of the case-study (˜550,000) because it has a greater kiln diameter than the reference, therefore, a larger computational domain.

The average absorber panel temperature at the maximum kiln shell temperature is used as the grid independence criterion through the methodology proposed in [22] which uses the fine-grid convergence index, %*GCI*, that indicates the numerical uncertainty of the solution, understood as the statistically independence of the result to the used mesh. Accordingly, the lower its value, the lesser the uncertainty. Once applied to the solution portrayed in Fig. 3, the encountered $\%GCI = 0.3\%$ for the reference and $\%GCI = 0.04\%$ for the cross-validation case-study, suggest that there is almost no uncertainty in the solution due to the used mesh.

Cross-validation variables such as the total heat flow emitted by the kiln shell, the radiation part of it and the average temperature of the absorber panel are calculated and recorded in Table 3. Indicators like the relative mean absolute difference, *RMAD*, and the coefficient of variation of the root mean square deviation, %*CV*(*RMSD*), are used for comparison. *RMAD*, as shown in Equation 2, allows to directly obtain the absolute variation between the value of a calculated variable and a fixed reference while the %*CV*(*RMSD*) parameter, calculated in Equation 3, compares point by point the temperature distribution along the length of the absorber panel between the reference and the cross-validation case-study. It is found that for the 0.36 m average element size grid both indicators performed well, that is, lesser or close to a 5% variation for all the inspected variables. In Equation 2 and 3, Y_i is the value of the calculated variable and Y_{ref} refers to the reference value. n is the number of compared points and $\overline{y}_i$ is the arithmetic average of the calculated variable.

$$\%\mathrm{RMAD} = ABS\left(\frac{Y_i - Y_{ref}}{Y_{ref}}\right)x100 \tag{2}$$

$$\%\mathrm{CV(RSMD)} = \frac{\sqrt{\frac{1}{n}\sum_{i=1}^{n}\left(Y_i - Y_{ref}\right)^2}}{\overline{y}_i}x100 \tag{3}$$

Table 2
Simulation monitors and absolute convergence criteria.

Monitors	Absolute criteria
Continuity	1E−04
x-velocity	1E−04
y-velocity	1E−04
energy	1E−08
k	1E−06
Omega	1E−06
Lift Coefficient	Flat
Drag Coefficient	Flat
#Iterations (max)	5000

4. Effect of positioning parameters

Once the cross-validation is successfully accomplished, it is in the best interest of the analysis to explore the effect of various location parameters such as: (1) the panel relative position to the vertical axis in degrees, (2) the separation from the kiln surface and (3) the arrangement of a vortex breaker at the tips of the panel. This analysis is carried out to select a configuration that improves the radiation waste-heat harvesting amount and quality, in terms of the average temperature of the absorber panel.

4.1. Relative position to the vertical axis

The maximum temperature achievable by the panel is directly related to the quality of the waste heat that can be used later. The heat transfer mechanisms that operate between the kiln shell and the panel are radiation between the surfaces and convection with the medium. Considering that the incident radiation depends solely on the geometric parameters of the surfaces for the *S2S* model and that it is a constant 90° span panel, the view factors do not vary significantly, therefore, the incident radiation remains relatively constant. However, when heat transfer by convection is assessed, it promptly appears that the relative position of the absorber panel to the vertical axis influences the greater or lower cooling rate of its surface. In this sense, it is understood that there is a position in which the highest temperature can be reached and that it is in turn parametrised by the separation with the kiln shell. In Fig. 4 it is depicted the average temperature of the absorber panel when the kiln shell temperature is held at its maximum, $T_{max} = 375$ °C. It is found that the peak temperature for the arc absorber when separated 0.3 m ($T = 226$ °C) and 0.7 m ($T = 216$ °C) from the kiln shell occurs at 105° and 95° from the vertical axis, respectively. The location of said peak temperature differs due to the air flow in between surfaces, and if such a flow is not obstructed by the panel, there is a greater cooling effect. Such an obstruction takes place first, in degrees from the vertical axis, when the panel is located farther from the kiln shell.

4.2. Separation from the kiln shell

The average by separation of the kiln shell to the vertical axis incident heat flow to the absorber panel without vortex breaker, per 5 m long section, is used to evaluate the influence of the absorber separation from the kiln surface. As it is found in Fig. 5 the highest incident heat flow of 190 kW occurs when the panel is separated 0.7 m from the kiln shell. However, there is a reason for that maximum, and it is found in the trade-off between panel area, which increases with the separation allowing a larger capture of the emitted radiation, and the cooling effect of the air flow which exerts an influence in the surface temperature,

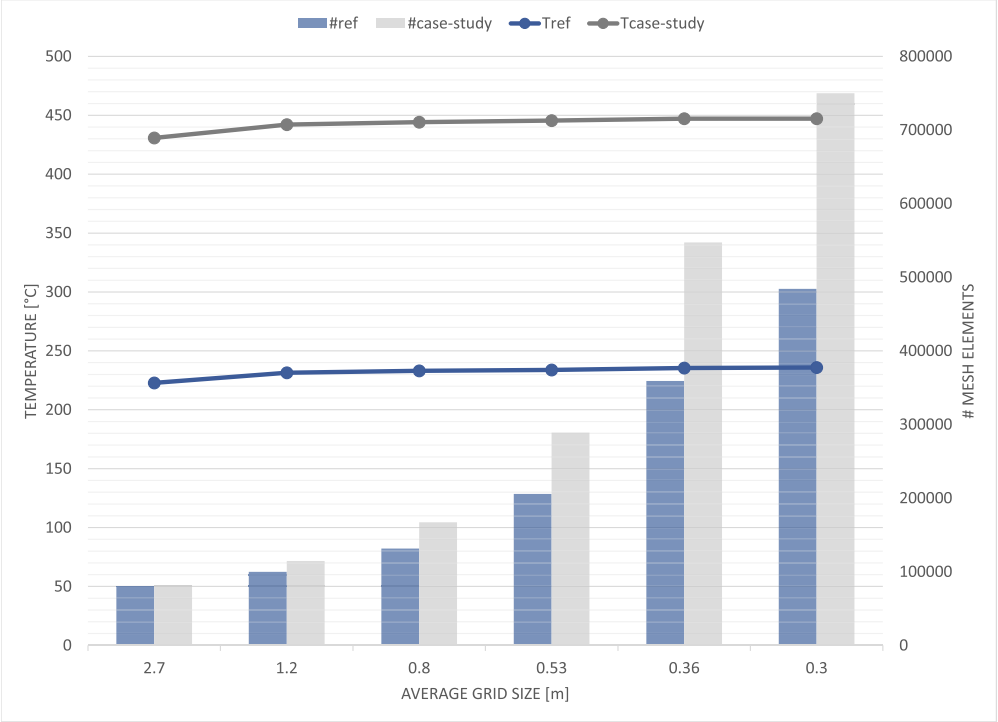

Fig. 3. Grid independence curves for the reference, in blue, and the case-study for cross-validation, in grey. (For interpretation of the references to colour in this figure legend, the reader is referred to the web version of this article.)

Table 3
Cross-validation variables and comparison indicators.

Surface	Variable	Reference [12]	Cross-validation	% RMAD	%CV RMSE
Kiln Shell	Tmax [°C]	500		–	–
	Total Heat Flow [kW]	230.44	223.49	3.02%	–
	Radiation Heat Flow [kW]	183.26	173.68	5.23%	–
Absorber Panel	T [°C]	520.15	509.03	2.14%	2.53%

therefore, in its ability to emit or receive radiation. The blue line in Fig. 5 portraits the complementary curve to the incident radiation to the absorber panel, that is, the energy lost as convection and radiation from the kiln surface that could not be recovered. This chart also includes the total heat flow emitted from the kiln shell and its shares of radiation (~83%) and convection (~17%), which are in accordance in magnitude with the results presented in [12]. It becomes clear that radiation is the leading mechanism of heat transfer between the surfaces, however, the effect of the vortex breaker is clearly marked, despite being a very small percentage concerning the total heat emitted by convection since only a small amount of convective losses occur when used. The relative position to the vertical axis has little to no effect in the heat flow estimation and variations are contained within a 5%. As long as the area of the panel offers a positive effect on radiation capture, it must be considered counterproductive in the sense of eventual construction and costs. For this reason, it is also desired to know at the minimum possible installation distance, in this case, 0.3 m separation from the kiln shell which would be the available heat flow, that is, 177 kW.

4.3. *Vortex breaker installation*

A vortex breaker, *VB*, is nothing else than a deflector plate, as shown in Fig. 2, that diverts the airflow in between the kiln shell and the absorber panel to avoid it from cooling them down. Such a simple device should keep the losses due to convection as low as possible, then, favouring the heat transfer by radiation. Although useful at first sight, such a plate or sweeper should not come in direct contact with the kiln surface due to safety reasons. Therefore, its length must be a fraction of the separation of the panel. In this work a half length separation, 0.35 m *VB* is installed to an absorber panel located at 0.7 m from the kiln shell. In Figs. 4 and 5 it is portrayed the behaviour of such a *VB*-Panel in terms of average temperature and incident heat flow per 5 m length section. The temperature of the panel increases from $T = 216$ °C to $T = 224$ °C when *VBs* are installed, confirming the reduction of convective losses, making the 0.7 m separation panel peak temperature almost the same as the 0.3 m one, even displacing the peak location to 105°. Despite the incipient yet positive effect on the incident heat flow, a 2 kW increase, and the average temperature of the absorber panel, 8 °C raise, because of this being a steady-state analysis, the abrupt changes that may be generated in convection losses product of wind variations are unknown. Hence, *VB* implementation is suggested in the eventual case of construction.

5. Waste heat recovery potential

Until this section, the temperature of the kiln shell is sustained at its maximum, $T = 375$ °C to tune up the CFD simulations. Nonetheless, the temperature of the kiln shell is averaged by 5 m section and varies along with the kiln length as shown in Fig. 6, all kiln shell temperatures were measured using a Raytek infrared pyrometer suitable to a 30–600 °C range. Such a variation implicates a change in the incident heat flow and the average temperature of the absorber panel, depending on its separation to the shell. Fig. 6 summarises the average temperature achieved by the 90° span panel while in Fig. 7 it is presented the incident heat flow. It appears that the drop in the incident heat flow its linked to the drop in the actual temperatures of the absorber panel and the kiln shell, which may be explained due to the presence of external cooling fans in the first sections of the kiln surface.

Taking into account the dimensions of the kiln, it would be

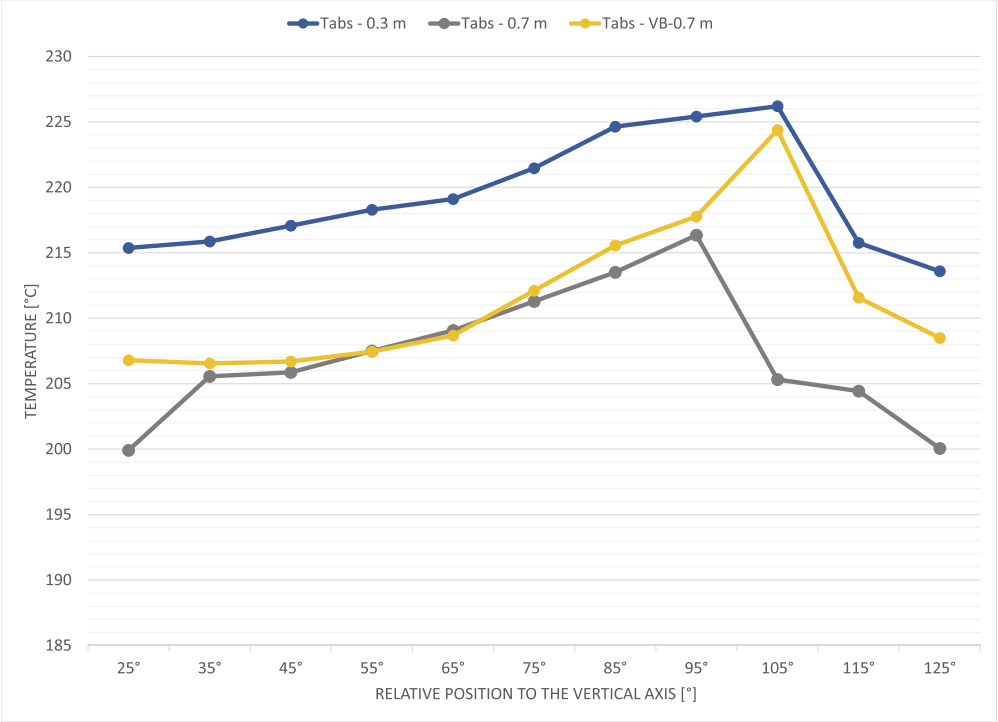

Fig. 4. Influence of the relative position to the vertical axis on the absorber panel temperature. Kiln shell temperature is held at $T_{max} = 375$ °C.

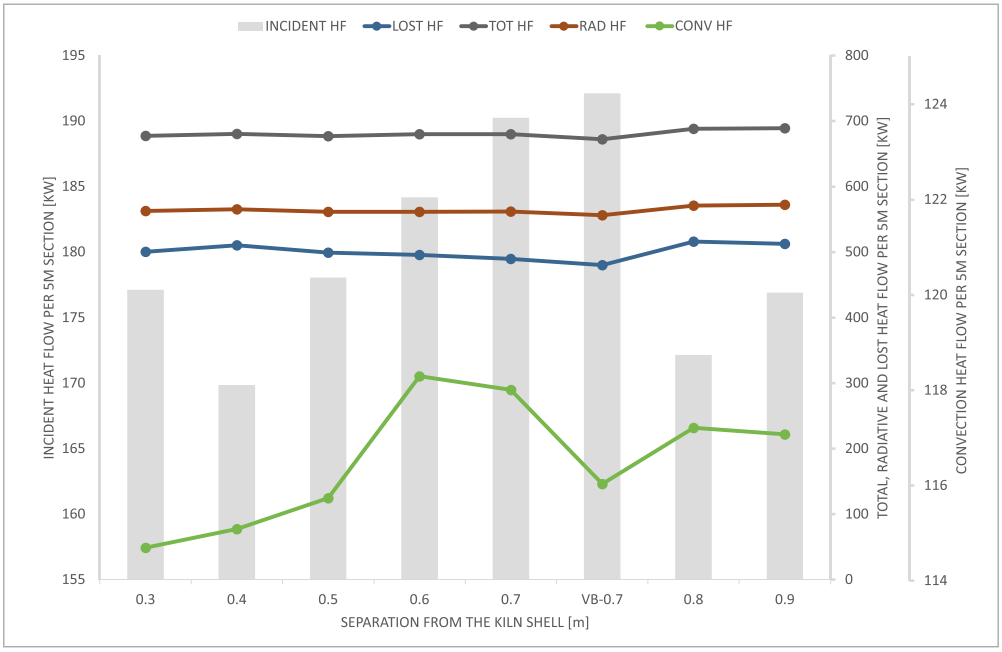

Fig. 5. Influence of the separation from the kiln shell on the absorber panel incident radiation heat flow, and the total, radiative, convective and lost heat flow from the kiln shell. Kiln shell temperature is held at $T_{max} = 375$ °C.

impractical to access the radiation from the entire exposed surface, so it is necessary to establish a limit based on the length in which the arrangement of the panels must be placed. Such a limit is associated with the sections that require further active cooling, that is, where the kiln shell could potentially surpass the maximum allowable temperature of the construction material. Seeing that the kiln shell is currently operating without issues, such a maximum temperature is fixed at $T = 375$ °C. Dotted lines and areas in Figs. 6 and 7 correspond to the potential temperatures and incident heat flow to the panel if the first sections of the kiln shell were operating at maximum temperature. Said assumption actually seeks to dismiss the need for an external cooling fan but for standby safety reasons. Removing the need of such devices could bring potential savings in the electricity consumption of the cement plant that can't be measured accurately in this work.

The kiln shell temperature tends to be higher in the flame zone than in the remaining length of the kiln as appreciated in Fig. 6. Such a trend has been described in terms of the inner kiln temperature and can be verified in [23,24,8,25]. Having said so, fixing the extension of the

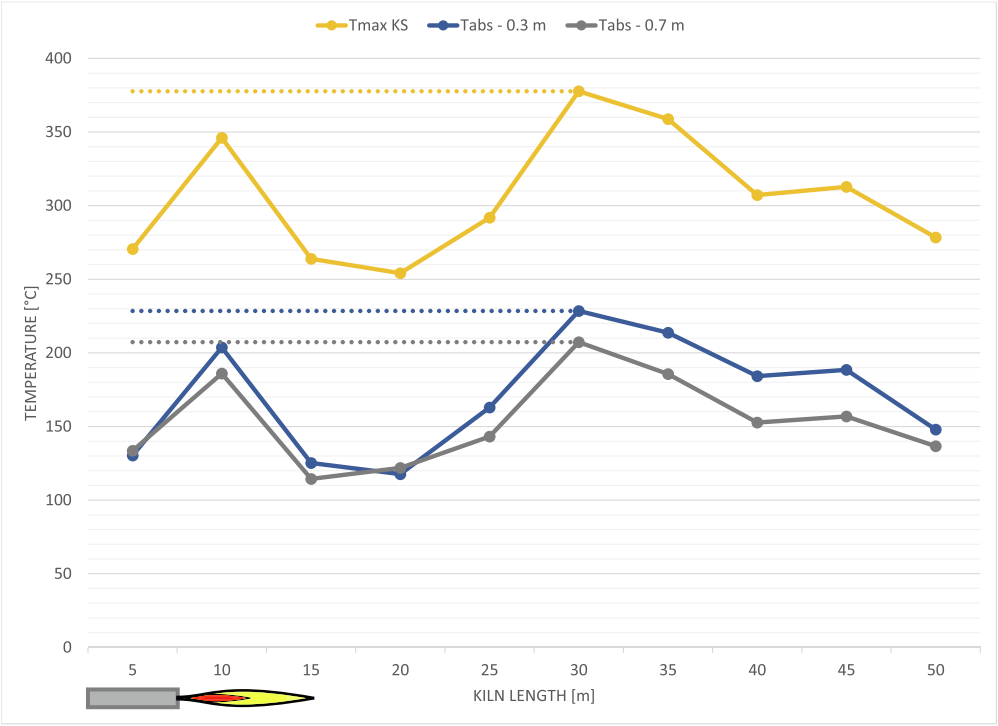

Fig. 6. Maximum temperature of the kiln shell and absorber panel along the kiln length. Dotted lines refers to potential the temperature of the first sections if no cooling fans were installed. Burner flame enters at 0 m of kiln length.

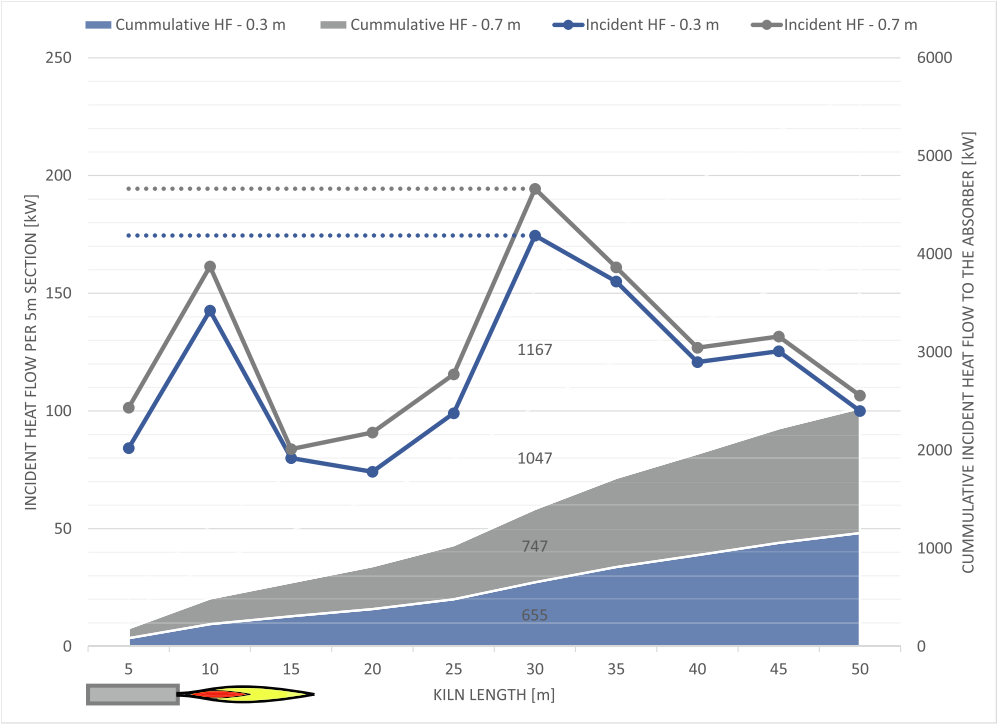

Fig. 7. Incident heat flow to the absorber panel along the kiln length. Dotted lines and areas correspond to the potential values achieved if no cooling fans were installed. Burner flame enters at 0 m of kiln length.

absorber panels up to 30 m of the kiln length, it is possible to capture an incident heat flow of 655–747 kW with current panel temperatures and up to 1047–1167 kW in the case of the potential achievable temperatures if the cooling fans are dismissed when a 90° span panel is used. As explained in Section 4.2, it is possible to capture more radiation with the panel separated 0.7 m from the shell.

Using a fixed 90° span for the absorber panel is convenient to speed up CFD simulations, however, it is not a physical constraint, moreover, it places a case in which losses due to convection are somewhat higher than those occurring if a larger obstruction to the airflow is placed in

between the panel and the shell. Also, it is an obvious remark that arranging a larger absorber surface could increase the incident radiation heat flow. For these reasons, in Fig. 8, it is portrayed the achievable temperatures of the absorber panel when located at 105° from the vertical axis (position at which the peak absorber temperature is achieved at 0.3 m separation and when *VB* are used) for an increasing span, starting in 90° and until it reaches a full 360° annulus, resembling the one in [13]. The incident heat flux on the panel increases with the absorber span, thus, for a 0.7 m separation from the shell, a 90° span absorber receives 1167 kW; a 180° one, 2427 kW; and a 270°, 3622 kW. However, the maximum heat recovery, 4980 kW, occurs with a span of 360°. For such a span it is also found the maximum temperature, which is 240 °C. Such heat and temperature are the ones to be used as input in the Recuperated ORC to generate electricity. In case the complete annulus absorber represents an obstruction to the kiln's maintenance operations, the possibility of dividing it into sections that operate in parallel should be considered. It also explores using a smaller span absorber, allowing the safe and smooth operation of the equipment.

6. Recuperated organic Rankine cycle for electricity generation

The incident heat flow encountered in Section 5 for the 360° span absorber panel at 30 m kiln length, separated 0.7 m from the kiln shell is the one to be used as input to the power cycle. That is, 4980 kW of heat entering to a Recuperated ORC working on CycloPentane. Working fluid selection and operation parameters as well as the equations used to model the energy, exergy and costing indicators are widely explained in a previous work [26]. However, in this case the evaporator which is unconventional, one side radiation, one side fluid, is modelled as a counter current, shell and tube heat exchanger where the heat source is assumed to be hot air entering at the film temperature between the absorber panel temperature $T = 240$ °C and the temperature of the leaving air, $T = 180$ °C. Then, the overall coefficient of heat transfer is set in 25 W/m^{2}K, value treated as a design parameter that is in relation to that predicted by [11,13], 21–31 W/m^{2}K, for the external surface of a panel that operates under similar conditions. Calculations done through this approach are expected to be conservative both in terms of required heat transfer area of the exchanger and costs. Any further refinement in this topic could be addressed in a future work.

In Table 4 are compiled some relevant indicators of the cycle performance. It is to note that the cycle delivers 864.25 kW of net work with a thermal efficiency of η_{th}=17.35% and an exergetic efficiency of η_{exg}=48.62%. The total exergy destroyed by the cycle, $I_{tot} = 843.71$ kW, is distributed among its components as shown in Fig. 9. Exergy destruction takes place mainly in the evaporator, 41%, and condenser, 39%. This occurs due to the high temperature gradient between the working fluid and the heat sinks whether it is the heat source or the cooling water. The required heat transfer area estimated for the evaporator is 3506.891 m^2 while the actual area of the absorber, based on geometry calculations, is 490.1 m^2 and 565.5 m^2 for panels separated 0.3 m and 0.7 m from the shell. The gap between the two, required heat transfer area and actual absorber area, must be supplied through

Table 4
Performance indicators for @180 °C Recuperated ORC operation.

T @180 °C	Cyclo-Pentane Recuperated
η_{carnot} [%]	24.82%
η_{th} [%]	17.35%
η_{exg} [%]	48.62%
I_{tot} [kW]	843.71
EDF [–]	0.98
VFR [–]	12.13
SP [m]	0.10
P_{evap} [bar]	16
T_{evap} [°C]	170
P_{cond} [bar]	1.43
Q_{in} [kW]	4980
W_{pump} [kW]	30.51
$W_{turbine}$ [kW]	894.75
W_{net} [kW]	864.25

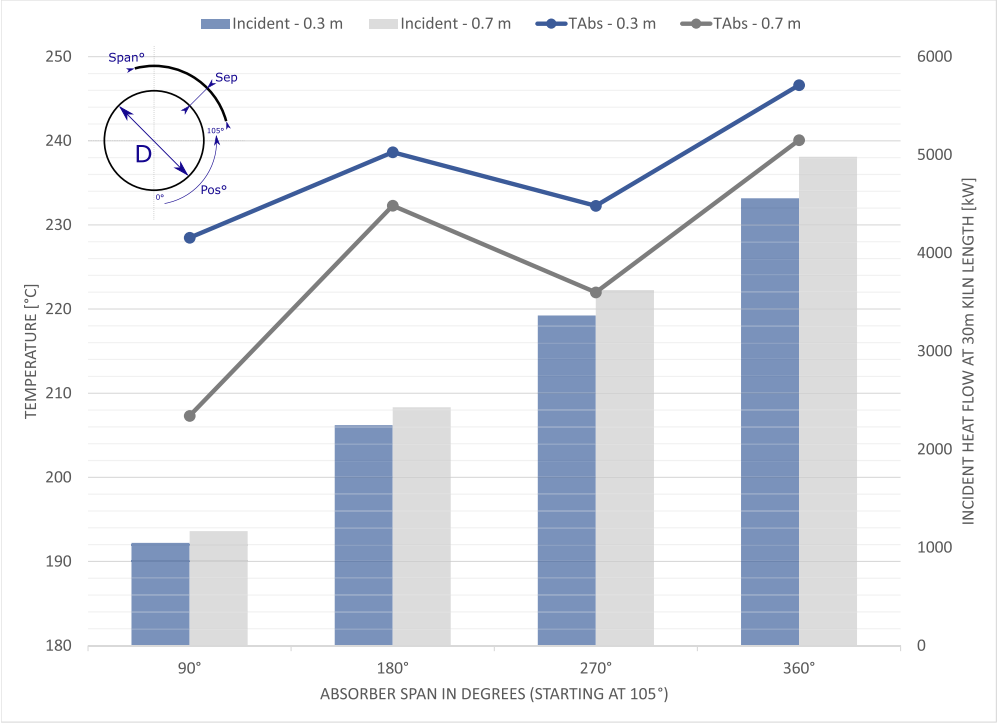

Fig. 8. Incident heat flow at 30 m kiln length and average temperature of the absorber panel vs the absorber span. In the top left corner it is a miniature of the setup. Panel span starts at 105° from the vertical axis.

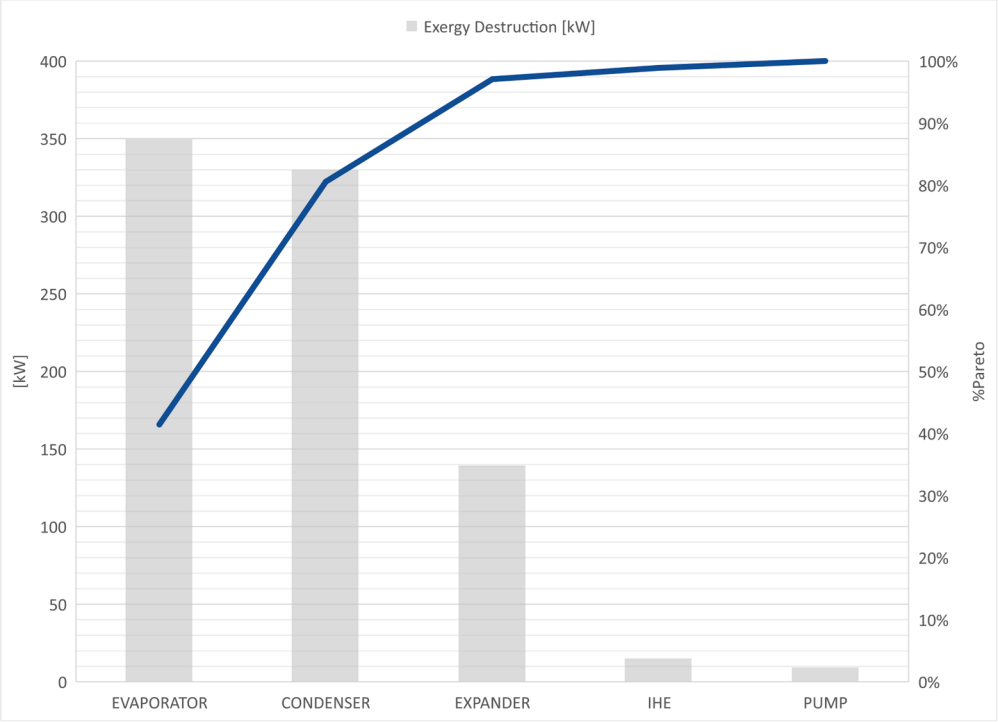

Fig. 9. Exergy destruction by component and Pareto line for the Recuperated ORC.

extended surfaces, like fins, and/or improving the overall heat transfer coefficient, using novel methodologies of radiation capture, like the use of heat pipes as seen in [27].

7. Economic performance

Net present value, *NPV*, is the selected economic parameter used to decide if the evaluated waste heat recovery system is profitable or not. In this sense, only positive values are going to be considered. Despite presenting useful information, *NPV* is not enough to describe the behaviour of the investment, therefore, the total capital cost of the investment which raises up to 6.06 MUSD, the rate of return, %*i*, the payback time, *PB*, and the average unit cost of electricity, *c*, are used to evaluate the economic performance of the Recuperated ORC once it is coupled to the absorber panel. Fig. 10 compiles the aforementioned economic parameters as a function of %*i* allowing to contextualise the

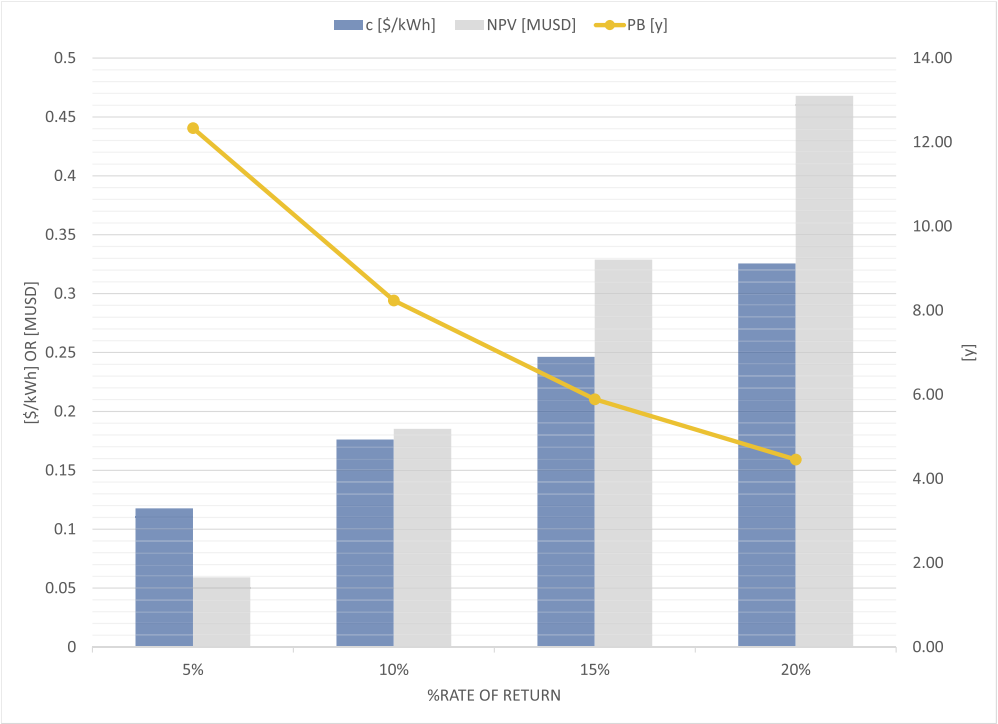

Fig. 10. Net present value, *NPV*, payback time, *PB* and average unit cost of electricity, *c*, vs rate of return, %*i*.

proposed recovery system as more or less profitable depending on the sale price of electricity in the place where it is to be installed, that is, the cost of electricity at an industrial level in the country where the kiln operates.

Once the information in Figs. 10 and 11 is contrasted, it is easy to say that the proposed recovery system makes sense, in terms of *NPV*, in most of those countries. However, since profitability is associated with the sale price of electricity, the rate of return achievable is much higher where market electricity price for the industrial sector are up to c_e = 0.35 $/kWh, e.g., as observed in some of the Latin Amerincan and Caribbean countries in Fig. 11 [28].

Such a return on the investment could peak to 20% in the best of cases, corresponding to a *NPV* close to 0.47 MUSD and a *PB* as low as 4.5 years. As for implementing a solution of this type in other parts of the world, Japan draws attention due to the cost of electricity that would allow a return close to 10% with a corresponding *NPV* of 0.19 MUSD and a *PB* of 8.2 years. The case of Europe is uneven, there are many countries where an investment of this type would be feasible, but with very low returns, in the order of 5%, which could anchor an implementation project to the need to self-generate electricity, for example, depending on whether there is or not the adequate interconnection with the grid. Despite this, there are still countries with high electricity tariffs, like Italy, where the return on investment could be close to 10%, similar to the case of Japan.

8. Conclusions

The geometric parameters of an absorber panel to capture the radiation emitted by a rotary kiln surface were determined through CFD simulations. Once the influence of each of them was explored in Section 4, it was found that the appropriate combination consisted of an annulus that extends 30 m of the length of the rotary kiln and is 0.7 m apart from its shell. This setup promotes the highest possible amount of heat capture, including the one which is usually dissipated by cooling fans in the first sections of the kiln, as well as the quality of the recovered heat in terms of the absorber temperature, which rises to $T = 240$ °C. Such a temperature is achieved due to the decrease in heat losses by convection as the airflow between the kiln shell and the panel is obstructed when compared to a 90° span absorber. The use of vortex breakers at the ends of the panel is recommended for applications of a span lesser than the full annulus as it fulfils this same purpose of obstructing the inflow of air.

The feasibility of implementing a waste heat recovery system based on the capture of radiation emitted from the surface of a rotary kiln is evaluated by coupling CFD analysis and modelling of processes, that is, material, energy, and exergy balances. It is found a potential heat recovery of up to 4980 kW of heat which are usable for generating 864.25 kW_e of electricity, corresponding to 16.6 MJ_e per tonne of clinker production, through a Recuperated ORC that operates with CycloPentane at 180 °C, with a thermal efficiency of η_{th} = 17.35% and an exergetic efficiency of η_{exg} = 48.62%. The economic performance of a waste heat recovery alternative like this is tied to the price of electric energy for the industrial sector of the place where the rotary kiln operates. In this way, the best candidates are those with the highest electricity costs. Industrial tariffs are selected instead of household ones because the consumption of the generated power should take place first inside the production facility. Such an assumption leads to a conservative approach to economics since the best candidates are those with the highest electricity costs and household prices tend to be higher than industrial ones. Specifically, the Latin American and Caribbean market, where the return on investment could reach values of even 20% in the best of cases with an *NPV* close to 0.47 MUSD and a *PB* as low as 4.5 years.

CRediT authorship contribution statement

José J. Fierro: Validation, Investigation, Software, Investigation, Writing - review & editing. **César Nieto-Londoño:** Conceptualization, Investigation, Methodology, Supervision, Project administration, Funding acquisition, Writing - review & editing. **Ana Escudero-Atehortua:** Conceptualization, Methodology, Writing - review & editing. **Mauricio Giraldo:** Conceptualization, Methodology, Supervision, Writing - review & editing. **Hussam Jouhara:** Conceptualization, Methodology, Supervision, Project administration, Funding acquisition,

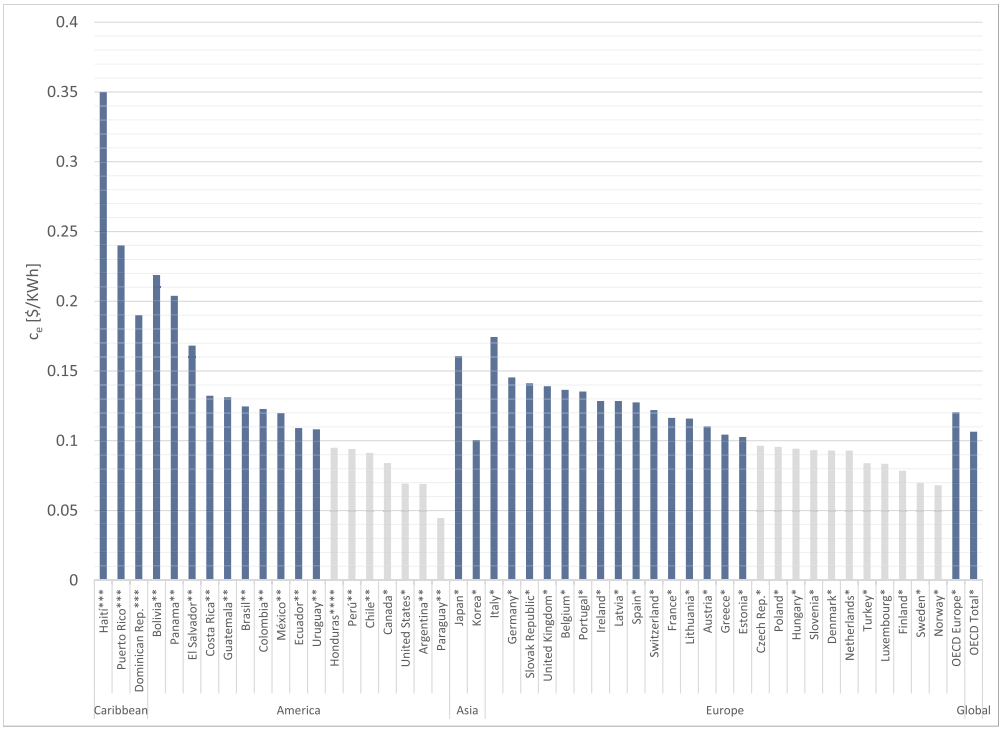

Fig. 11. Electricity price at industrial level for selected countries. In blue, countries with electricity prices exceeding 0.1 $/kWh. *[29] **[30] *** [28,31,32] ****[33].

Writing - review & editing. **Luiz C. Wrobel:** Conceptualization, Methodology, Supervision, Writing - review & editing.

Declaration of Competing Interest

The authors declare that they have no known competing financial interests or personal relationships that could have appeared to influence the work reported in this paper.

Acknowledgements

This research is funded by the The Royal Academy of Engineering through the Newton-Caldas Fund IAPP18-19\218 project that provides a framework where industry and academic institutions from Colombia and the UK collaborate in heat recovery in large industrial systems.

References

[1] N.A. Madlool, R. Saidur, N.A. Rahim, M.R. Islam, M.S. Hossian, An exergy analysis for cement industries: an overview, Renew. Sustain. Energy Rev. 16 (2012) 921–932.
[2] N.A. Madlool, R. Saidur, M.S. Hossain, N.A. Rahim, A critical review on energy use and savings in the cement industries, Renew. Sustain. Energy Rev. 15 (2011) 2042–2060.
[3] N.A. Madlool, R. Saidur, N.A. Rahim, M. Kamalisarvestani, An overview of energy savings measures for cement industries, Renew. Sustain. Energy Rev. 19 (2013) 18–29.
[4] H. Jouhara, N. Khordehgah, S. Almahmoud, B. Delpech, A. Chauhan, S.A. Tassou, Waste heat recovery technologies and applications, Therm. Sci. Eng. Prog. (2018).
[5] H. Jouhara, A. Żabnieńska-Góra, N. Khordehgah, D. Ahmad, T. Lipinski, Latent thermal energy storage technologies and applications: a review, Int. J. Thermofluids 5–6 (2020), 100039.
[6] J. Ke, N. Zheng, D. Fridley, L. Price, N. Zhou, Potential energy savings and CO2 emissions reduction of China's cement industry, Energy Policy 45 (2012) 739–751.
[7] A. Atmaca, R. Yumrutaş, Analysis of the parameters affecting energy consumption of a rotary kiln in cement industry, Appl. Therm. Eng. 66 (2014) 435–444.
[8] S. Sadighi, M. Shirvani, A. Ahmad, Rotary cement kiln coating estimator: integrated modelling of kiln with shell temperature measurement, Can. J. Chem. Eng. 89 (1) (2011) 116–125.
[9] S. Wirtz, C. Pieper, F. Buss, M. Schiemann, S. Schaefer, V. Scherer, Impact of coating layers in rotary cement kilns: Numerical investigation with a blocked-off region approach for radiation and momentum, Therm. Sci. Eng. Prog. 15 (2020), 100429.
[10] C. Csernyei, A.G. Straatman, Numerical modeling of a rotary cement kiln with improvements to shell cooling, Int. J. Heat Mass Transfer 102 (2016) 610–621.
[11] Q. Yin, Q. Chen, W.J. Du, X.L. Ji, L. Cheng, Design requirements and performance optimization of waste heat recovery systems for rotary kilns, Int. J. Heat Mass Transfer 93 (2016) 1–8.
[12] M. Mirhosseini, A. Rezaniakolaei, L. Rosendahl, Numerical study on heat transfer to an arc absorber designed for a waste heat recovery system around a cement kiln, Energies 11 (3) (2018).
[13] M. Mirhosseini, A. Rezania, L. Rosendahl, Harvesting waste heat from cement kiln shell by thermoelectric system, Energy (2019) 358–369.
[14] M. Mirhosseini, A. Rezania, L. Rosendahl, Power optimization and economic evaluation of thermoelectric waste heat recovery system around a rotary cement kiln, J. Cleaner Prod. 232 (2019) 1321–1334.
[15] T. Johnson, J. Beer, Radiative heat transfer in furnaces: Further development of the zone method of analysis, Symposium (International) on Combustion, vol. 14, 1973, pp. 639–649.
[16] E. Khodabandeh, M. Ghaderi, A. Afzalabadi, A. Rouboa, A. Salarifard, Parametric study of heat transfer in an electric arc furnace and cooling system, Appl. Therm. Eng. 123 (2017) 1190–1200.
[17] N. Bohlooli Arkhazloo, Y. Bouissa, F. Bazdidi-Tehrani, M. Jadidi, J.-B. Morin, M. Jahazi, Experimental and unsteady CFD analyses of the heating process of large size forgings in a gas-fired furnace, Case Stud. Therm. Eng. 14 (2019) 100428.
[18] M. Potgieter, C. Bester, M. Bhamjee, Experimental and CFD investigation of a hybrid solar air heater, Sol. Energy 195 (2020) 413–428.
[19] S.-R. Yan, A. Golzar, M. Sharifpur, J.P. Meyer, D.-H. Liu, M. Afrand, Effect of U-shaped absorber tube on thermal-hydraulic performance and efficiency of two-fluid parabolic solar collector containing two-phase hybrid non-Newtonian nanofluids, Int. J. Mech. Sci. 185 (2020), 105832.
[20] Q. Schmid, E. Hachem, Y. Mesri, A versatile immersed surface-to-surface method for radiation exchange: Implementation and validation, Int. J. Heat Mass Transfer 134 (2019) 1091–1100.
[21] F.R. Menter, Two-equation eddy-viscosity turbulence models for engineering applications, AIAA J. 32 (1994) 1598–1605.
[22] I.B. Celik, U. Ghia, P.J. Roache, C.J. Freitas, H. Coleman, P.E. Raad, Procedure for estimation and reporting of uncertainty due to discretization in CFD applications, J. Fluids Eng. Trans. ASME 130 (7) (2008) 0780011–0780014.
[23] K. Mujumdar, V. Ranade, Simulation of rotary cement Kilns using a one-dimensional model, Chem. Eng. Res. Des. 84 (2006) 165–177.
[24] K.S. Mujumdar, K.V. Ganesh, S.B. Kulkarni, V.V. Ranade, Rotary cement Kiln simulator (RoCKS): integrated modeling of pre-heater, calciner, kiln and clinker cooler, Chem. Eng. Sci. 62 (9) (2007) 2590–2607.
[25] C. Csernyei, A.G. Straatman, Forced convective heat transfer on a horizontal circular cylinder due to multiple impinging circular jets, Appl. Therm. Eng. 105 (2016) 290–303.
[26] J.J. Fierro, A. Escudero-Atehortua, C. Nieto-Londoño, M. Giraldo, H. Jouhara, L. C. Wrobel, Evaluation of waste heat recovery technologies for the cement industry, Int. J. Thermofluids 7–8 (2020), 100040.
[27] H. Jouhara, S. Almahmoud, A. Chauhan, B. Delpech, G. Bianchi, S.A. Tassou, R. Llera, F. Lago, J.J. Arribas, Experimental and theoretical investigation of a flat heat pipe heat exchanger for waste heat recovery in the steel industry, Energy 141 (2017) 1928–1939.
[28] NREL (National Renewable Energy Laboratory); U.S. Department of Energy (DOE), "Energy Transition Initiative: Island Energy Snapshot – Haiti. DOE/GO-102015-4657," tech. rep., NREL (National Renewable Energy Laboratory), 2015.
[29] International Energy Agency (IEA), Energy Prices and Taxes for OECD Countries 2019. OECD Publishing, Paris, 2019.
[30] Osinergmin, Tarifas Eléctricas en Latinoamérica – 4to Trimestre de 2019, 2019.
[31] NREL (National Renewable Energy Laboratory), Energy Transition Initiative: Island Energy Snapshot – Puerto Rico. DOE/GO-102015-4583, tech. rep., NREL (National Renewable Ebergy Laboratory), 2015.
[32] NREL (National Renewable Energy Laboratory); U.S. Department of Energy (DOE), Energy Transition Initiative: Island Energy Snapshot – Dominican Republic. DOE/GO-102015-4661, tech. rep., NREL (National Renewable Energy Laboratory), 2015.
[33] CREE (Comisión reguladora de energía eléctrica), Estructura tarifaria que debe aplicar la ENEE para la facturación a partir del mes de julio de 2020 – Honduras.